Evidence-based Match-status-Aware Gait Recognition for Out-of-Gallery Gait Identification

Heming Du*, Chen Liu*, Ming Wang, Lincheng Li, Shunli Zhang†, and Xin Yu†

Abstract—Existing gait recognition methods typically identify individuals based on the similarity between probe and gallery samples. However, these methods often neglect the fact that the gallery may not contain identities corresponding to the probes, leading to incorrect recognition. To identify Out-of-Gallery (OOG) gait queries, we propose an Evidence-based Match-status-Aware Gait Recognition (EMA-GR) framework. Inspired by Evidential Deep Learning (EDL), EMA-GR is designed to quantify the uncertainty associated with the match status of recognition. Thus, EMA-GR identifies whether the probe has a counterpart in the gallery. Specifically, we adopt an evidence collector to gather match status evidence from a recognition result pair and parameterize a Dirichlet distribution over the gathered evidence, following the Dempster-Shafer Theory of Evidence (DST). We measure the uncertainty and predict the match status of the recognition results, and thus determine whether the probe is an OOG query. To the best of our knowledge, our method is the first attempt to tackle OOG queries in gait recognition. Moreover, EMA-GR is agnostic against gait recognition methods and improves the robustness against OOG queries. Extensive experiments demonstrate that our method achieves state-of-the-art performance on datasets with OOG queries, and can also generalize well to other identity-retrieval tasks. Importantly, our method surpasses existing state-of-the-art methods by a substantial margin, achieving a 51.26% improvement when the OOG query rate is around 50% on OUMVLP.

Index Terms—Gait Recognition, Out-of-Gallery

1 Introduction

Gait recognition, as an important biometric retrieval task, aims to identify people by their way of walking [1] and is widely used in security monitoring and forensics. Gait recognition is formulated as a retrieval task, where a query gait sequence, namely a probe, is compared to gait sequences from a gallery. The sequence from the gallery with the minimal distance to the probe will be regarded as a match, and finally, its identity will be assigned to the probe.

Existing gait recognition methods assume that there are always corresponding identities in the gallery set. However, in practice, this assumption often does not hold. Some probe queries possibly do not have their corresponding identities in the gallery, referred to as Out-of-Gallery (OOG) queries. Unfortunately, existing methods do not have a mechanism to address OOG cases. As shown in Figure 1(a), current methods still find an identity in the gallery even though there is actually no identity of the probe in the gallery, leading to erroneous results. Therefore, it is highly desirable to develop a gait recognition method that is able not only to find correct identities of In-Gallery (IG) queries but also to identify OOG queries.

In contrast to existing gait recognition approaches, in this work, we formulate gait recognition as an uncertainty-aware feature matching problem. We propose an Evidence-based Match-status-Aware Gait Recognition (EMA-GR) framework that can effectively address both IG and OOG queries. EMA-GR is agnostic against gait recognition methods and can adopt any existing gait recognition network as a feature extractor for a probe query and gallery sequences. Once we obtain the features of gait sequences, we will retrieve the gallery sequence feature that has a minimal distance from that of the probe. Unlike existing methods that directly assign the identity of the retrieved gallery sequence to the probe, we further determine whether the features of the probe query and the retrieved gallery sequence are from the same identity, as shown in Figure 1(b).

Specifically, we adopt a deep network as an evidence collector to measure the amount of support gathered from the probe and the gallery features in favor of it being classified into a certain

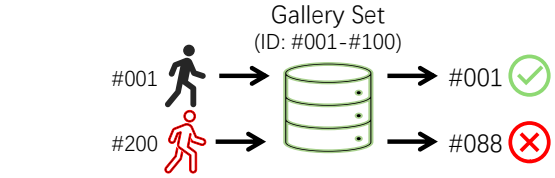

(a) Existing gait recognition methods

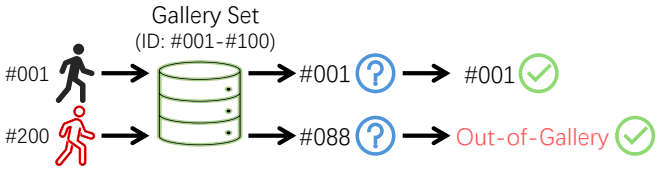

(b) The proposed Evidence-based Match-status-Aware Gait Recognition (EMA-GR) framework

Fig. 1. Comparison between traditional gait recognition framework and the proposed uncertainty-aware gait recognition framework when addressing In-Gallery (IG) and Out-of-Gallery (OOG) scenarios. Our framework can accurately recognize the OOG case.

- *Heming Du, Chen Liu, and Xin Yu were with the University of Queensland, Australia.*
- *Lincheng Li was with the Fuxi Lab, NetEase, Hangzhou, China.*
- *Ming Wang and Shunli Zhang were with the School of Software Engineering, Beijing Jiaotong University, Beijing, China.*
- ** Joint first authors*
- *† Xin Yu is the corresponding author. E-mail: xin.yu@uq.edu.au*

matching status, *i.e.*, matching or non-matching. Inspired by hard mining strategies, we design a query pair construction strategy to train the evidence collector. We combine the features with matched or unmatched identities into paired features for the evidence collector training. However, since the distribution of the features of the probe query and the gallery sequence retrieved in practice may fall outside the intervals trained by the evidence collector, it can lead to inaccuracies in the predictions. Therefore, it becomes essential to estimate uncertainty concurrently with predicting match status.

Inspired by Evidential Deep Learning (EDL), we adopt the Dempster-Shafer Theory of Evidence (DST) [2] to assign belief masses to a possible status based on collected evidence. To be specific, we utilize the evidence-parameterized Dirichlet distribution to assign belief masses, following the theory of Subjective Logic [3]. Unlike the evidence for one possible state, a belief mass can be assigned to any possible state of the frame, including the whole frame itself. By assigning the belief mass to the entire frame, every class can be assigned with the belief mass equally. In other words, unlike evidence that supports only one opinion about a match status, converting the collected evidence to belief masses allows our network to estimate the uncertainty of the prediction and thus express another opinion: "*I do not know*". Therefore, EMA-GR reflects the mass assignment of the input features and their uncertainty in the feature space under different conditions, including the IG and OOG query scenarios. As a result, EMA-GR provides a mechanism for detecting OOG probes. Once we obtain the Dirichlet distribution parameterized over the input features, we can apply it to examine whether a pair of retrieved gaits is from the same person and how confident our prediction is. As a result, our model predicts three scores: a matching score, a non-matching score and an uncertainty score. Based on the three scores, we are able to determine IG and OOG queries.

Extensive experiments demonstrate that our method achieves state-of-the-art performance in gait recognition with OOG queries. Importantly, our method outperforms the state-of-the-art method, *i.e.*, DyGait [4], by a large margin of 51.26% when the rate of OOG queries is 50% on one of the largest gait recognition datasets OUMVLP [5]. Our main contributions are summarized as follows:

- We propose a novel uncertainty-aware gait recognition model that can tackle both In-Gallery (IG) and Out-of-Gallery (OOG) queries in a unified framework. To the best of our knowledge, we are the first to address OOG cases for gait recognition.
- We model the uncertainty of the retrieved identity by applying the theory of evidential deep learning to represent the probability density.
- Our framework is agnostic against gait recognition backbones. It can be adopted by existing methods with minimal effort to address OOG queries, thus significantly improving the robustness of existing methods.

2 Related Work

Gait recognition aims to learn discriminative feature representations from people's skeletons or silhouettes for identification purposes [6], [7], [8], [9], [10], [11], [12]. Its objective is to obtain the identity information for a probe sample from the gallery. To achieve this goal, many studies focus on improving the feature extraction capability of the model. These methods can be categorized into three classes, *i.e.*, model-based methods, pose-based methods, and silhouette-based methods. Model-based methods are designed to extract features from RGB sequences, such as shapes, view angles, and postures [13], [14], [15]. Pose-based methods extract 2D poses or 3D poses of human bodies to obtain discriminative feature representations [16], [17], [18], [19]. Silhouette-based methods generate feature representations by aggregating all temporal information of a gait sequence [20], [21], [22], [23], [24], [25], [26], [27], [28], [29], [30], [31], [32], [33], [34], [35], [36], [37], [38], [39]. Although the above methods obtain high recognition accuracy, they often neglect the fact that a probe might be an Out-of-Gallery (OOG) sample, which does not have counterparts within the gallery. When such probes are exhibited, current methods would fail and cannot discern the absence of matching identities in the gallery. This is because they do not have a mechanism to handle OOG queries. To the best of our knowledge, our work is the first attempt to address the OOG query scenario in gait recognition.

Furthermore, many other recognition tasks, such as vehicle and human re-identification [40], [41], [42], as well as face recognition [43], [44], also follow a very similar recognition paradigm as gait recognition. Consequently, they encounter the same challenges posed by OOG queries. Our proposed method can be readily integrated into these tasks to enhance their recognition robustness against OOG queries, thus avoiding incorrect identity assignments. In addition, our method does not need to re-train the backbone networks, significantly facilitating the adaptation of existing networks to handle OOG queries.

Additionally, open-set recognition methods [45], [46] have been proposed to address the Out-of-Distribution (OOD) problem in recognition. These methods aim to classify the known classes while labeling all OOD samples to one unknown class. The distinction between our task and open-set recognition lies in the fact that all our probe samples are unseen during training. The most significant difference, however, is that our objective is not to identify OOD samples that do not belong to the training data but rather to ascertain whether a given probe is absent from the gallery. Therefore, the open-set recognition methods cannot be used for our task.

3 Uncertainty-aware Gait Recognition Framework

3.1 Gait Recognition Revisit

Existing gait recognition methods follow a standard paradigm, which can be divided into three steps: (i) Designing and training a gait recognition network. The gait recognition network can be trained with various losses to achieve strong feature extraction capability. (ii) Extracting features. Once the gait recognition network has been trained, it extracts features from a sequence sampled from the probe and gallery sets. Here, we denote $\mathbb{Q} = \{q_1, q_2, ..., q_M\}$ as all the probe features from the probe set and $\mathbb{G} = \{g_1, g_2, ..., g_N\}$ as all the gallery features from the gallery set, where q_i is i-th probe feature, g_j is the j-th gallery feature, and M and N indicate the number of the probe samples and gallery samples, respectively. (iii) Identifying probes based on the distance to the gallery features. We compute the distance between a probe feature q_i and all the gallery features. For a probe feature q_i, its distances with respect to all the gallery features can be represented as $\mathbb{D}_i = \{D(q_i, g_1), D(q_i, g_2), ..., D(q_i, g_Q)\}$, where D indicates the Euclidean distance in our experiments. Subsequently, we find the minimum distance in $\mathbb{D}_i$. Suppose

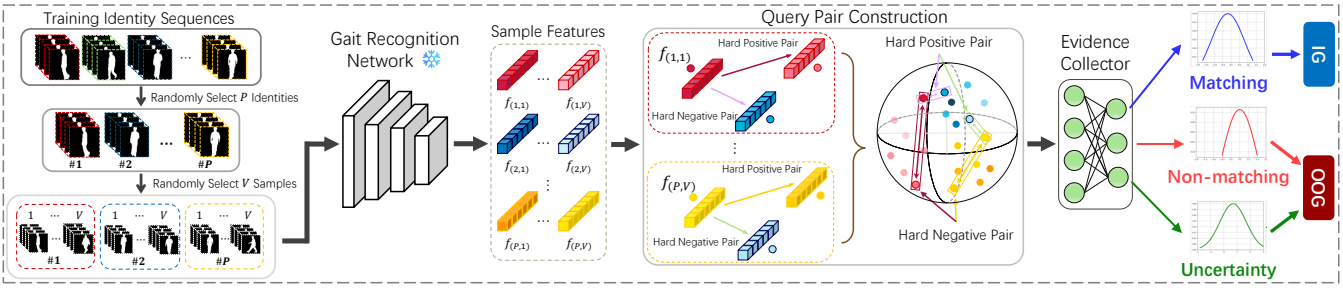

Fig. 2. Overview of the uncertainty-aware gait recognition framework. We first utilize existing backbones to extract features and then construct hard positive and negative feature pairs to train our evidence collector. By Dirichlet-based evidence learning, our method is able to predict matching, non-matching and uncertainty scores of a pair of the probe feature and the retrieved feature. As a result, our method is able to determine whether they are from the same identity. Note that our method does not need to re-train the backbone networks and thus can be easily applied to different backbones and other similar tasks.

$D(q_i, g_j)$ is the minimum value in $\mathbb{D}_i$, and then the identity of g_j will be assigned to the probe i.

However, in step (iii), conventional gait recognition methods neglect the fact there might be no matching identity in the gallery. Although $D(q_i, g_j)$ is minimum, the identity j should not be assigned to the probe i. When a probe does not have a counterpart identity in the gallery, we refer to it as an Out-of-Gallery (OOG) query, and a probe with matching identities is referred to as an In-Gallery (IG) query. To address both IG and OOG queries in a unified framework, we present an uncertainty-aware gait recognition method, as illustrated in Figure 2.

3.2 Dirichlet-based Evidence Learning

To distinguish IG and OOG queries in a unified framework, we model the probability distribution of the matching uncertainty based on the gathered evidence. Previous methods estimate prediction variance or uncertainty through dropout [47], [48], [49], [50], ensembling [51], [52] or other sampling approaches [53], [54]. However, this stream of work often relies on expensive sampling operations, and it is hard to apply them to feature-matching tasks since the probe and gallery features are often fixed.

In contrast, Bayesian inference offers a distinct advantage by enabling the estimation of uncertainty without the need for sampling. Bayesian inference methods [55], [56] place prior distributions over deep models. For example, Evidential Deep Learning (EDL) [3] and Prior Networks [57], [58] effectively apply Dirichlet priors over discrete classification predictions to provide robust uncertainty estimation.

Given an input feature $\boldsymbol{x}$, EDL first uses an evidence collector to generate the evidence $\boldsymbol{e} = \{e_k | k = 1, \ldots, K\}$, where K is the number of classes and e_k denotes the evidence of the k-th class. Based on the Subjective Logic theory [3], the evidence $\boldsymbol{e}$ corresponds to a Dirichlet distribution parameterized by $\boldsymbol{\alpha} = \{\alpha_k | k = 1, \ldots, K\}$, where $\alpha_k = e_k + 1$. A Dirichlet distribution is a probability density function for all the possible values of a probability mass function $\boldsymbol{p}$, and can be represented as:

$$\mathbf{D}(\boldsymbol{p} \mid \boldsymbol{\alpha}) = \begin{cases} \frac{1}{B(\boldsymbol{\alpha})} \prod_{i=1}^{K} p_i^{\alpha_i - 1} & \text{for } \boldsymbol{p} \in \mathcal{S}_K, \\ 0 & \text{otherwise}, \end{cases} \tag{1}$$

where $\mathcal{S}_K = \left\{ \boldsymbol{p} \mid \sum_{i=1}^{K} p_i = 1 \text{ and } 0 \le p_1, \ldots, p_K \le 1 \right\}$ is the K-dimensional unit simplex, and $B(\alpha)$ is the K-dimensional multinomial beta function [59]. Here, p_k is the expected probability for the k-th class and is calculated as $p_k = \frac{\alpha_k}{S}$, where $S = \sum_{i=1}^{K} \alpha_i$.

We denote the ground-truth label of $\boldsymbol{x}$ is $\boldsymbol{y}$ that is a K-dimensional one-hot vector with $y_i = 1$ and $y_k = 0$ for all $k \neq i$. Mean Square Error (MSE) is employed to measure the differences between the estimated class probabilities and the ground truth. It can be expressed as follows:

$$\begin{aligned} \mathcal{L}_m(\Theta) &= \int \|\boldsymbol{y} - \boldsymbol{p}\|_2^2 \, \mathbf{D}(\boldsymbol{p} \mid \boldsymbol{\alpha}) \\ &= \sum_{i=1}^{K} \left(y_i^2 - 2 y_i \mathbb{E}\left[p_i\right] + \mathbb{E}\left[p_i^2\right] \right), \end{aligned} \tag{2}$$

where $\mathbb{E}$ indicates the expectation operation.

Furthermore, if an input feature cannot be correctly classified, its evidence ideally should shrink to zero. In other words, the Dirichlet distribution will be a uniform Dirichlet distribution. To this end, Sensoy *et al.* [3] introduce a Kullback-Leibler (KL) divergence term. As a result, the total loss function is represented as:

$$\mathcal{L}(\Theta) = \mathcal{L}_m(\Theta) + \lambda_t KL\left[\mathbf{D}\left(\boldsymbol{p} \mid \tilde{\boldsymbol{\alpha}}\right) \| \mathbf{D}\left(\boldsymbol{p} \mid \langle 1, \ldots, 1 \rangle\right)\right], \tag{3}$$

where $\lambda_t = \min(1.0, t/10) \in [0, 1]$ is the annealing coefficient. $\mathbf{D}\left(\boldsymbol{p} \mid \langle 1, \ldots, 1 \rangle\right)$ indicates a uniform Dirichlet distribution, t is the index of the current training iteration, and $\tilde{\boldsymbol{\alpha}} = \boldsymbol{y} + (1 - \boldsymbol{y}) \odot \boldsymbol{\alpha}$ is the Dirichlet parameters after the removal of the non-misleading evidence from predicted parameters $\boldsymbol{\alpha}$ for the input feature $\boldsymbol{x}$.

3.3 Uncertainty Modeling for Gait Recognition

As aforementioned, the premise that the gallery must contain an identity corresponding to the probe sample is considerably difficult to satisfy in practice, and OOG query cases may more likely happen if the gallery size is limited. Therefore, a mechanism to tackle OOG gait recognition is highly desirable.

A straightforward approach to address this problem is to develop a binary classifier. This classifier determines whether a probe sample and a gallery sample, which exhibits the minimum distance to the probe feature, share the same identity. Here, the errors from the gait recognition networks should not affect the classifier performance as the adopted networks already achieve appealing performance on the gait feature representation. Using the simple classifier, the result of each retrieval can be formulated as follows:

$$Y = \begin{cases} OOG & F_c(q_i, g_j) \le 0.5, \\ IG & F_c(q_i, g_j) > 0.5, \end{cases} \tag{4}$$

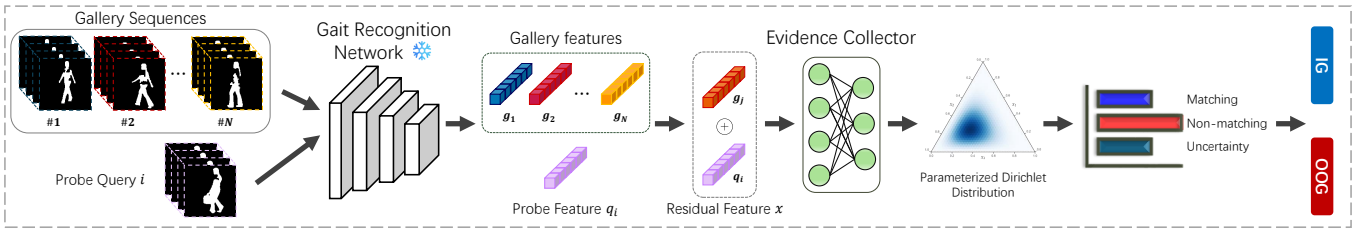

Fig. 3. Inference for the uncertainty-aware gait recognition framework. Given a probe feature q_i, we first search for a gallery feature g_j that has the minimum distance of q_i. Then, the combined feature is processed through the evidence collector to determine whether the probe is an IG and OOG query.

where Y is the framework output. *OOG* indicates the input probe feature q_i and gallery feature g_j are from different identities. *IG* represents the input probe feature q_i and gallery feature g_j are from the same identity. $F_c(\cdot)$ denotes the binary classifier that takes a probe feature and a gallery feature as input. Unfortunately, a simple binary classifier tends to output an over-confident erroneous prediction especially when an OOG query is fed into it. Hence, a classifier would fail to detect the OOG query, and thus the gait recognition methods would assign incorrect identities to probes.

To address this problem, we introduce the theory of EDL [3] into current gait recognition methods and then model the uncertainty of whether the query and retrieved features are from the same identity. The EDL theory is built on the Dempster-Shafer Theory of Evidence (DST), a generalization of the Bayesian theory to subjective probabilities [60]. To be specific, EDL assigns belief masses, *e.g.*, probabilities, to a set of mutually exclusive labels, *e.g.*, class labels for a sample. A belief mass can be assigned to any subset of a frame [60], including the whole frame itself. Here, the frame refers to the possible labels for a sample. Different from traditional binary classification, we can introduce a label "I do not know" into the frame, representing the uncertainty of a given sample based on the theoretical framework of EDL. To formulate the belief mass assignments, Subjective Logic theory (SL) [3] is an effective tool. Specifically, SL can formalize the belief assignments over a frame of discernment via a Dirichlet distribution. Thus, SL allows us to employ the principles of evidential theory to quantify the belief masses and uncertainty.

Driven by SL, we propose an uncertainty-aware gait recognition framework that enables us to recognize IG and OOG queries in a unified framework, as shown in Figure 2. In order to apply the uncertainty modeling of SL to our method, we first employ a gait recognition network to retrieve a gallery feature that has the minimum distance to a probe feature. Then, we compute the feature discrepancy between the probe and gallery features, called *residual feature*. Given the residual features, we aim to identify whether a query corresponds to an IG or OOG sample. Instead of directly assessing the similarity between the probe and every gallery sample, we opt to examine the distribution of residual features. This approach allows us to estimate the uncertainty of the probe without the computational burden of detailed gallery feature distribution modeling.

Modeling the gallery distribution implicitly via a discriminator will degenerate into the case of learning a simple classifier, which has been demonstrated ineffective for the gait recognition problem. In contrast, we consider $K = 2$ mutually exclusive singletons, *i.e.*, *matching* and *non-matching*, by providing a belief mass b_k for each singleton based on SL. Therefore, the singleton space is significantly smaller than the number of identities in the gallery set and simplifies the classification process. We assign belief masses b_1 and b_2, respectively, which represent the subjective probabilities of matching and non-matching pairs, alongside an overall uncertainty mass μ. The mass values are non-negative and collectively sum to unity, and can be expressed as follows:

$$\mu + \sum_{k=1}^{K} b_k = 1. \tag{5}$$

The retrieval result is determined by:

$$Y = \begin{cases} OOG & b_2 + \mu \geq b_1, \\ IG & b_2 + \mu < b_1. \end{cases} \tag{6}$$

When the prediction score of the matching class b_1 is higher than the sum of the score of the non-matching class b_2 and the uncertainty score, we believe the retrieved identity should be assigned to the probe. Otherwise, we will discard the retrieved identity as the probe sample could be an OOG query. Thanks to the uncertainty modeling of SL, we can effectively refuse OOG queries without harming the overall recognition performance.

3.4 Evidence Collector Design

In Equation (5), the mass values of b_k and μ are derived from the evidence ($e_k \geq 0$) and the evidence will be used to determine the Dirichlet distribution and uncertainty. Based on EDL, the evidence is a measure of support collected from data in favor of a sample to be classified into a certain class. Therefore, we develop a simple Multi-Layer Perceptron (MLP), including two fully-connected (FC) layers, to collect the evidence. That means the output of MLP is the evidence $\boldsymbol{e} = \{e_k | k = 1, \ldots, K\}$. To ensure the value of the evidence is non-negative, we adopt the ReLU function to filter the negative value. Once we obtain evidence e_k, the belief mass b_k and uncertainty mass μ are expressed as:

$$b_k = \frac{e_k}{S} \quad \text{and} \quad \mu = \frac{K}{S}, \tag{7}$$

where $S = \sum_{i=1}^{K}(e_i + 1)$. According to SL, a belief mass assignment corresponds to a Dirichlet distribution with parameters $\alpha_k = e_k + 1$ and $S = \sum_{i=1}^{K} a_i$ is the Dirichlet strength. Equation (7) can be written as:

$$b_k = \frac{a_k - 1}{\sum_{i=1}^{K} a_i} \quad \text{and} \quad \mu = \frac{K}{\sum_{i=1}^{K} a_i}. \tag{8}$$

Equation (8) implies if the strength of a Dirichlet distribution or evidence is larger, the Dirichlet distribution is more concentrated and the uncertainty of the prediction will become smaller. At that point, the prediction of the network will be more reliable. If the

network predicts that the probe and the retrieved gallery sample share the same identity, as illustrated in Equation (6), the probe is likely to be an IG query. Otherwise, the probe might be considered as an OOG query. If evidence is lower (*i.e.*, the probabilities assigned to the two classes are small), the Dirichlet distribution will be flatter and the uncertainty of the prediction will be higher. Thus, the input might come from an OOG query.

3.5 Query Pair Construction

Our uncertainty-aware classification model aims to determine whether a pair of retrieved features are from the same identity or not. To train our classification model, we need to simulate the testing input. For this purpose, we construct pairs of samples, including positive and negative pairs. To be specific, a positive pair is obtained by sampling different sequences from the same identity, while we sample two sequences from different identities to construct a negative pair.

A simple strategy is to construct positive and negative pairs by randomly selecting two samples from the training set. Here, negative pairs are randomly chosen from two identities and positive pairs are randomly selected within the same identity. Even though we balance the number of positive and negative pairs, we find the network cannot effectively classify hard negative pairs. This is because the constructed pairs contain numerous simple cases that can be distinguished easily. In other words, our model does not have many chances to learn uncertain cases during training.

Inspired by the hard mining strategies, we construct the hardest positive and the hardest negative pairs within each training batch and thus enforce our model to classify highly uncertain samples. To be specific, we first randomly select P identities from the training set and then randomly choose V samples from each identity. Therefore, a total of $P \times V$ samples can be selected. Denote $\mathbb{I} = \{f_{(1,1)}, f_{(1,2)}, \ldots, f_{(i,j)}, \ldots, f_{(P,V)}\}$ be the features of all selected samples. (i, j) indicates the j-th samples of the i-th identity. For the feature $f_{(i,j)}$, we can calculate the Euclidean distance between $f_{(i,j)}$ and each feature in $\mathbb{I}$. Finally, the hardest positive pair can be constructed as $< f_{(i,j)}, f_{(i,q)} >$, where $f_{(i,q)}$ has the maximum distance with the feature $f_{(i,j)}$ for all samples in the i-th identity. The hardest negative pair can be constructed as $< f_{(i,j)}, f_{(v,w)} >$, where $f_{(v,w)}$ has the minimum distance with the feature $f_{(i,j)}$ and $v \neq i$. For all the features of I in the batch, we can totally generate $P \times V$ hardest positive pairs and $P \times V$ hardest negative pairs.

3.6 Inference

The inference stage of the uncertainty-aware gait recognition framework is shown in Figure 3. We first use a gait backbone to extract all the probe and gallery features. Recall that $\mathbb{Q} = \{q_1, q_2, ..., q_M\}$ denotes the probe features from the probe set and $\mathbb{G} = \{g_1, g_2, ..., g_N\}$ represents the gallery features from the gallery set. For each probe feature q_i, we compute the distances between q_i and all the gallery features and then find the gallery feature g_j that has the minimum distance to the probe.

Different from existing methods that assign the identity of g_j to the probe sample i, we utilize our uncertainty-aware gait recognition model to further determine whether the two features are from the same identity. To be specific, we compute the feature discrepancy between the two features. The feature discrepancy is then fed into our uncertainty-aware gait recognition model to generate evidence $\boldsymbol{e} = \{e_1, e_2\}$. From Equation (7), we can obtain the matching probability b_1, the non-matching probability b_2 and the uncertainty probability μ. Given the three probabilities, we can determine whether the probe sample i is an IG or OOG query based on Equation (6).

4 Experiments

4.1 Dataset

We evaluate the effectiveness of our method on three gait recognition benchmarks OUMVLP [5], CASIA-B [61], and Gait3D [10]. Moreover, to verify the applicability of our method to other tasks, we also conduct experiments on other similar benchmarks, such as vehicle re-identification benchmark VERI-Wild [62], [63] and synthetic person-identification benchmark VC-Clothes [64]. The details of these datasets are depicted as follows.

OUMVLP [5] is a large-scale gait dataset. It includes 10,307 subjects, each of which contains a gallery set and a probe set. Each subject in a set is collected from 14 views ($0°$–$90°$ and $180°$–$270°$ with a sampling interval of $15°$). In this work, we use the evaluation protocol presented in [65], [66], [67] to verify the effectiveness of the proposed uncertainty-aware gait recognition framework. Under the default evaluation protocol, 7% of the probes are OOG queries, which brings a challenge to the state-of-the-art methods. In addition, we randomly remove some gallery sets of subjects to construct more severe OOG query scenarios.

CASIA-B [61] is one of the most popular gait datasets. It includes 124 subjects and about 1.3K sequences. Each subject is collected in sequences from 11 views ($0°, 18°, \ldots, 180°$). For each view, 10 groups of sequences are collected. In our experiments, the CASIA-B dataset is divided into three subsets: a training set, a query set, and a gallery set. To be specific, 74 IDs[1] are used to construct the training set, and the remaining 50 IDs are used as the query and gallery sets. We select one image from each ID as the gallery set and the rest of the images as the query set. By randomly removing IDs from the gallery set, we construct various OOG query cases.

Gait3D [10] is a large-scale and in-the-wild dataset. It includes 4K subjects and 25K sequences captured by 39 surveillance cameras in the wild. In our experiments, the Gait3D dataset is divided into three subsets: a training set, a query set, and a gallery set. To be specific, 3K IDs[1] are used to construct the training set, and the remaining 1K IDs are used as the query and gallery sets. We select one image from each ID as the query set and the rest of the images as the gallery set. By removing IDs from the gallery set, we construct various OOG query cases. Note that, in the default evaluation protocol, 5% of the probes are OOG queries. Moreover, we randomly remove some subjects in the gallery set to construct more severe OOG query scenarios.

VERI-Wild [62], [63] is a large-scale dataset used for vehicle re-identification tasks. It includes 416,314 images captured by 174 surveillance cameras in the wild. In general, the VERI-Wild dataset is divided into three subsets: a training set, a query set, and a gallery set. We use the evaluation protocol as in [68], which includes three different settings, *i.e.*, Small-size Setting (SS), Medium-size Setting (MS) and Large-size Setting (LS). In the three settings, 3K IDs, 5K IDs and 10K IDs are used to construct the query and gallery sets, respectively. In each setting, we select one image from each ID as the gallery set and the rest of

1. Here, ID refers to identity. With a slight abuse of notation, we refer to ID as IG for simplicity.

TABLE 1
Rank-1 accuracy (%) on the OUMVLP dataset under different OOG percentages. The standard deviation is shown in parentheses. For a fair comparison, we join the backbones with different OOG detection strategies, *e.g.*, Naive CLS, Verification and Anomaly Detection. Here, in the default evaluation protocol, 7% of the probes are OOG queries.

Methods	OOG percentages					
	7%	15%	25%	35%	45%	55%
GaitSet	87.34	79.71	70.35	61.80	52.29	42.73
GaitSet + Naive CLS	88.43 (± 0.00)	83.09 (± 0.00)	76.94 (± 0.00)	71.86 (± 0.02)	67.00 (± 0.07)	63.28 (± 0.06)
GaitSet + Verification	87.37 (± 0.00)	80.53 (± 0.01)	72.26 (± 0.02)	64.85 (± 0.02)	56.83 (± 0.02)	49.22 (± 0.03)
GaitSet + Anomaly Detection	87.85 (± 0.00)	81.24 (± 0.03)	73.39 (± 0.03)	66.58 (± 0.02)	59.54 (± 0.06)	53.40 (± 0.06)
GaitSet + Ours	**88.14 (± 0.00)**	**86.64 (± 0.03)**	**85.16 (± 0.02)**	**84.26 (± 0.03)**	**83.84 (± 0.06)**	**84.09 (± 0.03)**
GaitPart	88.80	80.97	71.39	62.65	52.96	43.23
GaitPart + Naive CLS	90.38 (± 0.00)	85.78 (± 0.02)	80.64 (± 0.02)	76.49 (± 0.05)	72.71 (± 0.06)	70.05 (± 0.08)
GaitPart + Verification	88.72 (± 0.00)	81.88 (± 0.01)	73.65 (± 0.02)	66.37 (± 0.01)	58.54 (± 0.03)	51.16 (± 0.02)
GaitPart + Anomaly Detection	89.66 (± 0.00)	83.50 (± 0.01)	76.33 (± 0.01)	70.22 (± 0.02)	64.15 (± 0.11)	59.11 (± 0.10)
GaitPart + Ours	**89.88 (± 0.00)**	**88.41 (± 0.01)**	**86.96 (± 0.03)**	**86.03 (± 0.06)**	**85.53 (± 0.01)**	**85.68 (± 0.01)**
GaitGL	90.17	82.15	72.35	63.45	53.58	43.68
GaitGL + Naive CLS	92.27 (± 0.00)	88.81 (± 0.01)	84.99 (± 0.03)	82.02 (± 0.05)	79.51 (± 0.05)	77.87 (± 0.08)
GaitGL + Verification	90.47 (± 0.00)	83.06 (± 0.00)	74.14 (± 0.02)	66.19 (± 0.02)	57.67 (± 0.06)	49.52 (± 0.07)
GaitGL + Anomaly Detection	91.53 (± 0.00)	86.21 (± 0.02)	80.15 (± 0.05)	75.15 (± 0.06)	70.43 (± 0.05)	66.77 (± 0.09)
GaitGL + Ours	**91.52 (± 0.00)**	**90.27 (± 0.01)**	**89.03 (± 0.03)**	**88.21 (± 0.04)**	**87.82 (± 0.02)**	**87.87 (± 0.05)**
GaitBase	92.88	84.91	74.65	64.94	54.96	44.81
GaitBase + Naive CLS	96.35 (± 0.00)	92.47 (± 0.02)	88.21 (± 0.01)	84.90 (± 0.02)	82.01 (± 0.05)	80.26 (± 0.05)
GaitBase + Verification	97.24 (± 0.00)	94.74 (± 0.03)	92.02 (± 0.03)	89.80 (± 0.02)	87.76 (± 0.03)	86.32 (± 0.02)
GaitBase + Anomaly Detection	94.83 (± 0.00)	88.85 (± 0.01)	82.06 (± 0.04)	76.43 (± 0.02)	71.06 (± 0.05)	67.04 (± 0.07)
GaitBase + Ours	**98.63 (± 0.00)**	**97.48 (± 0.01)**	**96.33 (± 0.00)**	**95.50 (± 0.02)**	**94.93 (± 0.03)**	**94.73 (± 0.00)**
DyGait	92.94	84.96	74.68	64.97	54.98	44.82
DyGait + Naive CLS	97.30 (± 0.00)	94.48 (± 0.05)	91.51 (± 0.01)	89.29 (± 0.03)	87.48 (± 0.07)	86.61 (± 0.04)
DyGait + Verification	97.28 (± 0.00)	94.19 (± 0.06)	90.74 (± 0.05)	87.89 (± 0.05)	85.28 (± 0.06)	83.41 (± 0.08)
DyGait + Anomaly Detection	95.60 (± 0.00)	90.61 (± 0.05)	85.11 (± 0.04)	80.72 (± 0.07)	76.83 (± 0.02)	74.29 (± 0.04)
DyGait + Ours	**99.00 (± 0.00)**	**98.13 (± 0.04)**	**97.26 (± 0.01)**	**96.65 (± 0.02)**	**96.20 (± 0.03)**	**96.08 (± 0.02)**

the images as the probe set. By randomly removing IDs from the gallery set or probe set, we construct various OOG query cases.

VC-Clothes [64] is a synthetic person re-identification dataset. It includes 512 subjects, and each subject has 36 corresponding images. The dataset has been divided into two subsets: a training set and a testing set. Each set contains 256 IDs. In the inference stage, we randomly choose four images from each subject for the gallery set and the rest of the images are used in the probe set. Hence, the gallery and probe sets contain 1020 images and 8591 images, respectively.

4.2 Implementation Details

The proposed evidence collector is built on a multilayer perceptron (MLP), including two FC layers. For the OUMVLP dataset, we adopt five common gait recognition methods, GaitGL [67], GaitPart [66], GaitSet [65], OpenGait [69], and DyGait [4], as the backbones to extract gait features and evaluate the effectiveness of the proposed evidence collector. Since the feature sizes of the five backbones are different, we set the hidden layer size of our MLP to 544, 544, 768, 768, and 769, respectively. For the CASIA-B dataset [61], the MLP hidden layer size of five frameworks is set to 8192. For the Gait3D dataset [10], we also take the five frameworks as the backbones to extract gait features and evaluate the effectiveness of the proposed evidence collector. We set the hidden layer size of our MLP to 8192. For the VERI-Wild dataset [62], [63], BoT [70] is used as the backbone, and thus the hidden layer size of MLP of the uncertainty-aware classification model is set to 1024. For the VC-clothes dataset, we take CBN [71] as the backbone and the hidden layer size of MLP is set to 4096.

In Section 3.5, we design a query pair construction strategy to generate positive and negative sample pairs for the model training. The designed strategy is controlled by two hyper-parameters, P and V, which are fixed at 32 and 8, respectively, across all experiments. Meanwhile, the learning rate is initialized at 1×10^{-3} and undergoes a tenfold reduction every 10 iterations. Additionally, the total number of training iterations is set to 50 in all experimental settings for fair comparison.

Furthermore, we run each OOG percentage setting three times in order to demonstrate the robustness of our method against OOG queries. Specifically, in each OOG percentage setting, we randomly remove a certain percentage of the identities from the original gallery set to construct a different gallery set. Since we construct OOG queries on both OUMVLP [5], CASIA-B [61], and Gait3D [10] datasets, we will release all OOG configurations, along with the training and evaluation code, including checkpoints, to ensure reproducibility.

TABLE 2
Rank-1 accuracy (%) on the CASIA-B dataset under different OOG percentages. The standard deviation is shown in parentheses. For a fair comparison, we join the backbones with different OOG detection strategies, *e.g.*, Naive CLS, Verification and Anomaly Detection.

Methods	OOG percentages					
	0%	15%	25%	35%	45%	55%
GaitSet	91.81	79.39	70.92	63.23	53.22	42.53
GaitSet + Naive CLS	91.78 (± 0.00)	81.77 (± 0.87)	74.10 (± 1.06)	66.89 (± 1.46)	61.05 (± 1.98)	55.18 (± 0.62)
GaitSet + Verification	83.31 (± 0.00)	78.22 (± 0.55)	71.89 (± 0.48)	70.39 (± 1.12)	68.45 (± 1.76)	66.85 (± 1.59)
GaitSet + Anomaly Detection	91.72 (± 0.00)	81.69 (± 0.79)	74.78 (± 0.89)	68.17 (± 1.91)	62.30 (± 1.43)	55.34 (± 1.00)
GaitSet + Ours	**91.38 (± 0.00)**	**83.25 (± 1.13)**	**76.55 (± 0.77)**	**71.80 (± 1.80)**	**68.94 (± 3.62)**	**63.12 (± 2.25)**
GaitPart	92.61	80.16	72.19	63.63	53.81	44.20
GaitPart + Naive CLS	91.38 (± 0.00)	81.10 (± 0.75)	73.44 (± 1.16)	66.95 (± 0.22)	61.47 (± 1.23)	56.70 (± 1.13)
GaitPart + Verification	81.00 (± 0.00)	74.96 (± 0.79)	68.28 (± 0.80)	66.84 (± 1.25)	65.36 (± 1.42)	65.46 (± 0.92)
GaitPart + Anomaly Detection	91.59 (± 0.00)	79.49 (± 0.55)	70.95 (± 0.97)	63.04 (± 0.82)	55.59 (± 1.18)	49.45 (± 1.33)
GaitPart + Ours	**90.94 (± 0.00)**	**81.80 (± 0.37)**	**74.93 (± 0.64)**	**70.00(± 1.00)**	**66.22 (± 1.63)**	**61.88 (± 1.94)**
GaitGL	94.77	81.89	73.27	64.50	54.74	44.01
GaitGL + Naive CLS	94.47 (± 0.00)	85.10 (± 1.17)	77.27 (± 1.02)	71.71 (± 1.28)	66.38 (± 0.58)	59.90 (± 0.59)
GaitGL + Verification	32.00 (± 0.00)	41.62 (± 0.14)	47.98 (± 0.78)	54.79 (± 0.63)	61.42 (± 0.047	68.33 (± 0.60)
GaitGL + Anomaly Detection	94.77 (± 0.00)	83.55 (± 0.56)	74.91 (± 0.70)	66.62 (± 1.46)	58.58 (± 1.26)	48.93 (± 0.75)
GaitGL + Ours	**93.79 (± 0.00)**	**85.61 (± 1.08)**	**79.06 (± 0.92)**	**74.83 (± 1.52)**	**70.96 (± 0.61)**	**65.83 (± 0.27)**
GaitBase	96.01	82.97	74.11	64.44	54.64	44.82
GaitBase + Naive CLS	95.89 (± 0.00)	84.69 (± 0.29)	77.65 (± 1.29)	69.71 (± 0.54)	63.37 (± 1.80)	57.36 (± 0.65)
GaitBase + Verification	96.01 (± 0.00)	82.89 (± 0.57)	73.78 (± 0.66)	64.42 (± 0.65)	55.32 (± 0.15)	47.02 (± 1.06)
GaitBase + Anomaly Detection	95.89 (± 0.00)	84.36 (± 0.31)	77.05 (± 1.07)	68.75 (± 0.36)	62.10 (± 1.70)	55.44 (± 0.51)
GaitBase + Ours	**95.45 (± 0.00)**	**86.75 (± 0.75)**	**81.53 (± 1.36)**	**76.20 (± 0.69)**	**72.43 (± 2.45)**	**68.62 (± 2.78)**
DyGait	97.28	84.05	74.94	64.41	54.47	44.56
DyGait + Naive CLS	97.28 (± 0.00)	86.22 (± 0.32)	77.66 (± 0.31)	70.75 (± 0.88)	63.67 (± 0.75)	57.26 (± 1.02)
DyGait + Verification	42.53 (± 0.00)	50.95 (± 0.29)	56.66 (± 0.88)	62.23 (± 1.50)	67.79 (± 1.10)	73.88 (± 1.25)
DyGait + Anomaly Detection	97.28 (± 0.00)	86.23 (± 0.37)	77.68 (± 0.33)	70.46 (± 0.96)	63.16 (± 0.51)	56.29 (± 0.76)
DyGait + Ours	**95.76 (± 0.00)**	**89.38 (± 0.35)**	**85.06 (± 0.89)**	**83.36 (± 1.76)**	**81.66 (± 1.42)**	**77.98 (± 1.48)**

4.3 Comparisons with the State-of-the-Art

Evaluation on OUMVLP under different OOG percentages: We adopt our uncertainty-aware classification model with several state-of-the-art gait recognition models, including GaitGL [67], GaitPart [66], GaitSet [65], OpenGait [69], and DyGait [4] on the OUMVLP dataset, and compare their performance with and without employing our method. In the experiments, we run five gait recognition models on six test sets with different percentages of OOG samples. As indicated in Table 1, after introducing our method, all gait recognition models obtain improvements on the test sets with OOG samples. As the percentage of OOG samples increases in the test sets, we observe that existing methods suffer severe performance degradation. As expected, when the OOG query rate reaches 50%, the accuracy of these methods is reduced to nearly half of their original performance, with the accuracy of DyGait dropping from 92.94% to 44.82%. This implies that current gait recognition methods do not have the ability to detect OOG probes. In contrast, our uncertainty-aware classification model is able to identify OOG queries and thus avoids assigning gallery IDs to the probes. As a result, our method maintains high recognition accuracy while successfully recognizing OOG probes, indicating the effectiveness and superiority of the proposed method. Moreover, the small standard deviation of our results demonstrates the stability of our model in recognizing OOG samples.

Evaluation on CASIA-B under different OOG percentages: For the CASIA-B dataset, we also choose GaitGL [67], GaitPart [66], GaitSet [65], OpenGait [69], and DyGait [4] as our baseline algorithms. Table 2 presents the experimental results. It can be observed that our method leads to a slight decrease in performance when OOG samples are not present, with the accuracy of DyGait decreasing from 97.28% to 95.76%. This is because our method is designed to prioritize accuracy in identifying matching pairs, minimizing the risk of incorrect pairings. Consequently, our method achieves promising performance in all OOG scenarios. Specifically, the accuracy of DyGait without our uncertainty model decreases significantly as the percentage of OOG samples increases, with the accuracy of GaitGL dropping from 97.28% to 44.56%. Meanwhile, our method consistently outperforms the baseline in all six OOG percentages.

Evaluation on Gait3D under different OOG percentages: For the Gait3D dataset, we choose GaitGL [67], GaitPart [66], GaitSet [65], OpenGait [69], and DyGait [4] as our baseline backbones. Table 3 shows the experimental results. It can be observed that our method achieves a significant performance improvement in all cases. For instance, in the 55% OOG percentage, our method outperforms DyGait by 36.31%. Although our method still achieves a significant performance improvement in all OOG percentages, it suffers performance degradation in the 5% OOG percentage for GaitSet and GaitPart backbones. Since previous state-of-the-art methods cannot effectively extract discriminative features on the Gait3D dataset, their accuracy remains below 55%.

TABLE 3
Rank-1 accuracy (%) on the Gait3D dataset under different OOG percentages. The standard deviation is shown in parentheses. For a fair comparison, we join the backbones with different OOG detection strategies, *e.g.*, Naive CLS, Verification and Anomaly Detection. Note that, the default evaluation protocol contains 5% of the probes which are OOG queries.

Methods	OOG percentages					
	5%	15%	25%	35%	45%	55%
GaitSet	55.33	40.24	32.46	27.66	21.51	17.00
GaitSet + Naive CLS	54.27 (± 0.00)	43.26 (± 1.42)	40.12 (± 1.40)	41.59 (± 0.88)	43.67 (± 0.30)	45.72 (± 1.18)
GaitSet + Verification	55.33 (± 0.00)	42.36 (± 1.45)	34.38 (± 1.02)	29.79 (± 0.52)	26.41 (± 1.46)	24.46 (± 1.76)
GaitSet + Anomaly Detection	55.61 (± 0.00)	43.16 (± 0.94)	37.78 (± 0.73)	36.02 (± 1.02)	35.63 (± 0.48)	36.53 (± 0.97)
GaitSet + Ours	**51.20 (± 0.00)**	**39.92 (± 0.84)**	**38.99 (± 0.56)**	**41.82 (± 0.93)**	**46.36 (± 0.95)**	**51.33 (± 0.95)**
GaitPart	43.32	29.49	23.72	20.17	15.75	12.48
GaitPart + Naive CLS	39.09 (± 0.00)	30.86 (± 0.51)	31.54 (± 0.23)	33.33 (± 1.09)	37.01 (± 0.88)	38.97 (± 0.66)
GaitPart + Verification	43.41 (± 0.00)	30.93 (± 0.90)	24.94 (± 0.67)	21.61 (± 0.67)	19.24(± 1.10)	17.29 (± 0.92)
GaitPart + Anomaly Detection	40.63 (± 0.00)	30.58 (± 1.20)	29.10 (± 0.89)	29.26 (± 0.71)	30.89 (± 0.73)	30.93 (± 0.69)
GaitPart + Ours	**39.86 (± 0.00)**	**30.70 (± 0.84)**	**31.86 (± 0.32)**	**35.83 (± 0.55)**	**41.08 (± 0.71)**	**45.18 (± 1.53)**
GaitGL	73.77	56.48	48.41	40.44	31.69	24.78
GaitGL + Naive CLS	73.87 (± 0.00)	58.59 (± 0.39)	53.05 (± 0.57)	48.22 (± 0.36)	46.46 (± 0.91)	45.18 (± 1.41)
GaitGL + Verification	72.04 (± 0.00)	56.80 (± 0.12)	50.24 (± 0.68)	45.02 (± 0.70)	42.55 (± 1.01)	40.28 (± 1.01)
GaitGL + Anomaly Detection	73.77 (± 0.00)	57.79 (± 0.53)	50.75(± 0.87)	44.54 (± 0.36)	40.92 (± 1.60)	38.48 (± 1.00)
GaitGL + Ours	**74.15 (± 0.00)**	**59.49 (± 1.58)**	**56.06 (± 0.89)**	**53.40 (± 1.49)**	**54.05 (± 0.82)**	**55.00(± 0.80)**
GaitBase	75.02	57.15	47.74	40.82	34.48	27.56
GaitBase + Naive CLS	73.29 (± 0.00)	60.13 (± 1.44)	55.20 (± 1.30)	54.24(± 1.18)	55.30 (± 0.79)	57.05 (± 0.77)
GaitBase + Verification	74.92 (± 0.00)	59.39 (± 1.65)	49.88 (± 1.33)	42.26 (± 0.55)	36.40 (± 1.03)	32.46 (± 1.31)
GaitBase + Anomaly Detection	74.92 (± 0.00)	59.65 (± 1.69)	51.00 (± 1.23)	44.38 (± 0.47)	39.73 (± 0.53)	37.27(± 1.41)
GaitBase + Ours	**75.31 (± 0.00)**	**60.35 (± 1.11)**	**56.09 (± 1.26)**	**55.52 (± 1.54)**	**57.06 (± 0.75)**	**59.07 (± 0.14)**
DyGait	75.98	62.05	52.25	45.43	37.46	30.45
DyGait + Naive CLS	76.46 (± 0.00)	65.96 (± 0.92)	60.39 (± 1.45)	58.69 (± 0.96)	59.42 (± 0.83)	61.54 (± 0.16)
DyGait + Verification	72.62 (± 0.00)	62.18 (± 0.73)	56.51 (± 1.20)	54.43 (± 0.25)	53.66 (± 1.14)	53.92 (± 0.71)
DyGait + Anomaly Detection	76.17 (± 0.00)	64.90 (± 0.74)	58.05 (± 1.22)	54.14 (± 1.39)	52.42 (± 1.89)	53.44 (± 1.16)
DyGait + Ours	**76.27 (± 0.00)**	**66.92 (± 1.63)**	**62.91 (± 1.71)**	**62.76 (± 0.83)**	**64.48 (± 0.71)**	**66.76 (± 0.21)**

When the extracted features are not sufficiently discriminative, in handling IG queries, our method tends to be inaccurate. This is because, in such cases, the distance between a matching pair is large, leading to a higher risk. Meanwhile, our network prefers to accept matching pairs with minimal risk.

Evaluation on VERI-Wild and VC-Clothes under different OOG percentages: Although our model is designed to tackle OOG queries in gait recognition, it can be easily extended to other tasks, such as vehicle re-identification and person re-identification. To further verify the effectiveness of our method on other tasks, we conduct experiments on VERI-Wild [62], [63] and VC-Clothes [64].

For the VERI-Wild dataset, we choose the BoT framework [70] as our baseline algorithm. The experimental results are shown in Table 5. It can be observed that our method (BoT + Ours) achieves appealing performance in all cases. To be specific, our method achieves stable recognition accuracy for the five OOG percentages while outperforming the baseline method. In contrast, the accuracy of BoT without our uncertainty model decreases significantly as the percentage of OOG samples increases. For the VC-Clothes dataset, we employ the CBN framework [71] as our baseline algorithm. As indicated in Table 6, our methods achieve approximately more than 97% recognition accuracy in all the cases, *i.e.*, OOG percentage ranges from 15% to 55%. On the contrary, the recognition accuracy of CBN without our uncertainty model is 44.98% in the setting of 55% OOG samples. This is because the current methods cannot address OOG queries, and thus their methods only output erroneous recognition results. Note that, when we apply our method to the baseline methods, we do not need to re-train the baselines but treat them as off-the-shelf backbone networks. This also indicates that our method is able to effectively recognize matching feature pairs and OOG queries through its prediction and uncertainty modeling, thus demonstrating the superiority of our method to competing methods.

4.4 Ablation Study

To verify the effectiveness of the proposed components, *i.e.*, the uncertainty modeling and query construction, we conduct ablation studies on the OUMVLP dataset [5].

TABLE 4
Rank-1 accuracy (%) on the OUMVLP dataset under different OOG percentages. The standard deviation is shown in parentheses. For a fair comparison, we join the backbones with different OOG detection strategies, *e.g.*, Naive CLS, Verification and Anomaly Detection.

Methods	OOG percentages					
	7%	15%	25%	35%	45%	55%
GaitGL	90.17	82.15	72.35	63.45	53.58	43.68
GaitGL + Threshold=0.6	90.41 (± 0.00)	84.74 (± 0.01)	78.05 (± 0.03)	72.30 (± 0.03)	66.46 (± 0.12)	61.23 (± 0.12)
GaitGL + Threshold=0.7	73.08 (± 0.00)	74.21 (± 0.02)	75.72 (± 0.03)	77.24 (± 0.04)	79.21 (± 0.07)	81.35 (± 0.06)
GaitGL + Threshold=0.8	27.34 (± 0.00)	33.87 (± 0.02)	41.83 (± 0.02)	49.07 (± 0.00)	57.09 (± 0.03)	65.07 (± 0.05)
GaitGL + Threshold=0.9	9.42 (± 0.00)	17.56 (± 0.01)	27.52 (± 0.01)	36.57 (± 0.02)	46.56 (± 0.01)	56.51 (± 0.01)
GaitGL + Naive CLS	92.27 (± 0.00)	88.81 (± 0.01)	84.99 (± 0.03)	82.02 (± 0.05)	79.51 (± 0.05)	77.87 (± 0.08)
GaitGL + Verification	90.47 (± 0.00)	83.06 (± 0.00)	74.14 (± 0.02)	66.19 (± 0.02)	57.67 (± 0.06)	49.52 (± 0.07)
GaitGL + Anomaly Detection	74.07 (± 0.00)	75.63 (± 0.02)	77.58 (± 0.04)	79.42 (± 0.03)	81.57 (± 0.02)	83.79 (± 0.02)
GaitGL + Ours	**91.52 (± 0.00)**	**90.27 (± 0.01)**	**89.03 (± 0.03)**	**88.21 (± 0.04)**	**87.82 (± 0.02)**	**87.87 (± 0.05)**
DyGait	92.94	84.96	74.68	64.97	54.98	44.82
DyGait + Threshold=0.6	92.94 (± 0.00)	84.96 (± 0.00)	74.68 (± 0.00)	64.97 (± 0.00)	54.98 (± 0.00)	44.82 (± 0.00)
DyGait + Threshold=0.7	93.36 (± 0.00)	85.00 (± 0.01)	74.80 (± 0.02)	65.54 (± 0.03)	55.39 (± 0.01)	45.33 (± 0.02)
DyGait + Threshold=0.8	97.91 (± 0.00)	95.72 (± 0.06)	93.32 (± 0.04)	91.39 (± 0.02)	89.69 (± 0.05)	88.53 (± 0.04)
DyGait + Threshold=0.9	31.50 (± 0.00)	37.64 (± 0.03)	45.19 (± 0.02)	52.03 (± 0.05)	59.57 (± 0.03)	67.09 (± 0.05)
DyGait + Naive CLS	97.30 (± 0.00)	94.48 (± 0.05)	91.51 (± 0.01)	89.29 (± 0.03)	87.48 (± 0.07)	86.61 (± 0.04)
DyGait + Verification	97.28 (± 0.00)	94.19 (± 0.06)	90.74 (± 0.05)	87.89 (± 0.05)	85.28 (± 0.06)	83.41 (± 0.08)
DyGait + Anomaly Detection	95.60 (± 0.00)	90.61 (± 0.05)	85.11 (± 0.04)	80.72 (± 0.07)	76.83 (± 0.02)	74.29 (± 0.04)
DyGait + Ours	**99.00 (± 0.00)**	**98.13 (± 0.04)**	**97.26 (± 0.01)**	**96.65 (± 0.02)**	**96.20 (± 0.03)**	**96.08 (± 0.02)**

TABLE 5
Rank-1 accuracy (%) on the VERI-Wild dataset under different OOG percentages. The standard deviation is reported in parentheses. SS, MS and LS indicate 3K, 5K and 10K training IDs, respectively.

Setting	Methods	OOG percentages				
		15%	25%	35%	45%	55%
SS	BoT	74.07	66.02	57.86	49.40	40.90
	BoT + Naive CLS	69.26	66.76	64.81	63.25	62.82
	BoT + Verification	74.10	66.36	58.99	52.01	46.24
	BoT + Ours	**78.19**	**76.34**	**75.09**	**74.71**	**75.34**
MS	BoT	71.00	63.64	55.83	47.73	39.87
	BoT + Naive CLS	64.81	61.65	59.33	57.17	55.84
	BoT + Verification	70.85	63.34	55.86	48.17	41.04
	BoT + Ours	**73.70**	**70.85**	**68.97**	**67.65**	**67.36**
LS	BoT	65.58	58.65	51.54	44.15	36.82
	BoT + Naive CLS	59.25	56.28	53.39	50.99	49.15
	BoT + Verification	65.43	58.63	51.57	44.40	37.14
	BoT + Ours	**67.45**	**64.14**	**61.25**	**59.07**	**57.92**

TABLE 6
Rank-1 accuracy (%) on the VC-Clothes dataset under different OOG percentages. The standard deviation is reported in parentheses.

Methods	OOG percentages				
	15%	25%	35%	45%	55%
CBN	83.91	73.67	64.10	54.34	44.98
CBN + Verification	89.68	90.71	91.72	92.90	93.95
CBN + Threshold	87.96	80.93	75.74	72.00	69.17
CBN + Ours	**97.11**	**97.15**	**97.29**	**97.58**	**97.70**

4.4.1 Effectiveness of the Uncertainty Modeling

Since existing backbones cannot handle OOG cases, they cannot reach 100% accuracy in all OOG settings. For a fair comparison, we introduce different OOG detection strategies and join them with the gait backbone to construct baseline algorithms. As a result, the upper bound accuracy of the constructed baseline algorithms is 100%. The details of baseline algorithms are as follows:

Backbone + Naive CLS: An NN classifier is designed to classify whether two features are from the same identity or not. The classifier is trained on the constructed pairs using binary cross-entropy loss as the supervision. The difference between this classifier and our model is that our model has uncertainty modeling. Thus, our model not only classifies whether two features are from the same identity but also provides the uncertainty estimation of the prediction by a Dirichlet distribution parameterized over all the constructed training pairs, while a simple classifier only makes decisions based on its predicted labels since it only learns a classification boundary. As shown in Table 1, without any mechanism to distinguish OOG queries, the performance degrades as the number of OOG samples increases. Although a simple classifier slightly outperforms our method in the 7% OOG percentage, we can see that as the percentage of OOG queries increases, the performance of the simple classifier suffers significant degradation. This is

because a simple classifier tends to overfit the IG pairs. Thus, it may produce inaccurate predictions, when the input probe are OOG quires.

Backbone + Verification: Setting a similarity threshold is another straightforward way to address OOG cases. When the similarity between the probe and the closet sample from the gallery is smaller than the threshold, the probe will be regarded as an OOG query. In our cases, the threshold is calculated by Equal Error Rate (EER) from the verification setting. To be specific, we construct 20k gait pairs, including 10k paired samples and 10k unpaired samples. Then, we search for the best threshold leading to the lowest EER. Finally, the searched threshold is used to further determine whether two samples are from the same identity. We will release the constructed gait pairs for reproducibility. Table 1 shows that the verification-based methods address a few OOG cases, leading to a slight performance improvement. For example, in the 15% OOG setting, "DyGait + Verification" outperforms DyGait by 9.23% on OUMVLP. However, the verification-based methods cannot handle most OOG cases. This is because most OOG queries are hard samples. Here, "hard" means the OOG query is very similar to the closet sample from the gallery set. In other words, its similarity is higher than the given threshold, leading to erroneous results.

Backbone + Anomaly Detection: One-Class Novelty Detection [72] is proposed to address OOG cases in recognition. It aims to classify all OOG cases into a single class. Although it cannot be used directly in our task, we combine it with an NN classifier to detect our OOG cases. Specifically, we randomly construct IG and OOG feature pairs to train an NN classifier. The trained classifier is then employed in feature matching to determine whether the retrieved gait pairs have the same identity or not. As shown in Table 1, one-class novelty detection effectively addresses a few OOG cases. For example, "DyGait + Anomaly Detection" outperforms DyGait by 2.66% when the OOG query rate is 5% on OUMVLP. However, as the OOG rate increases to 45% and 55%, its performance declines significantly. This is because one-class novelty detection tends to classify an IG pair that has a large distance to OOG cases. As a result, the accuracy in low OOG percentage shows a significant decrease. In contrast, our method maintains recognition performance even though the OOG sample rate is more than 50%. Our method successfully identifies OOG queries and assigns correct identities to IG queries. We conduct experiments three times on different gallery sets. The small standard deviation values prove the stability of our method.

Impacts of different thresholds: For a fair comparison, we introduce different OOG detection strategies. One of our used strategies is to set a similarity threshold. If the similarity between the probe and the closet sample from the gallery is smaller than the threshold, the probe will be regarded as an OOG query. In this paper, we introduce a verification setting to automatically calculate the threshold. Obviously, the threshold can be set manually. Thus, we conduct experiments on OUMVLP by manually searching all thresholds. The experimental results are shown in Table 4. When the given threshold is lower than 0.6, the threshold-based method cannot detect any OOG cases. Thus, the accuracy in these threshold settings is the same as the accuracy using only the backbone. We also observe that a low threshold for GaitGL achieves appealing performance when the OOG percentage is less than 25%, but it cannot effectively address the condition with higher OOG percentages. In contrast, a high threshold achieves promising performance in high OOG percentages ($\geq$ 35%). For the DyGait backbone, we find that only "Threshold = 0.8" achieves promising performance, while other threshold settings lead to significant performance degradation.. These results indicate that it is difficult to choose a suitable threshold for different OOG percentages. Thus, the threshold-based methods are impractical. Furthermore, it can be found that our method outperforms the threshold-based methods in all OOG percentages and the recognition accuracy in all OOG percentages is stable. We believe that the proposed method is a more practical approach to addressing OOG queries in a real scene.

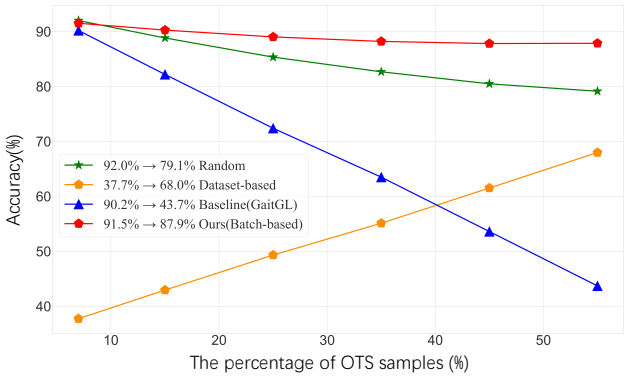

Fig. 4. Impacts of different query pair construction on training our model. We test the models with different percentages of OOG queries.

4.4.2 *Effectiveness of the Query Pair Construction*

We propose an OOG query pair construction that allows our network to grasp the idea of IG and OOG residual features. We also compare three different strategies: randomly selecting feature pairs, dataset-based hard negative and positive feature pairs, and batch-based hard negative and positive feature pairs. All experiments are conducted on OUMVLP and we take GaitGL as our backbone. As indicated in Figure 4, both random selection and batch-based hard negative and positive feature pair mining strategies improve the recognition performance on OOG cases in testing. Note that, as the percentage of the OOG queries increases, the performance of the model trained with randomly selected feature pairs decreases. This is mainly because this pair construction may not effectively capture the most uncertain cases for model training. The dataset-based mining strategy does not facilitate the representation of the distribution of the residual features. In most cases, the negative feature pairs from the dataset-based mining strategy are hard to classify, and thus our classifier will exert more effort to classify the negative pairs after training while sacrificing the classification accuracy of positive pairs. Mining in a batch-based pair will significantly improve the variety of training samples, thus leading to better recognition performance. Thanks to our feature pair construction, we can effectively capture the latent distribution of residual features, thus achieving accurate detection of OOG samples.

5 Discussion, Limitation and Extension

In this section, we further analyze the advantages and limitations of EMA-GR. Additionally, we extend our method to other tasks, *i.e.*, vehicle re-identification and person re-identification.

Performance of the default evaluation protocol: In this paper, we combine the backbone networks with different OOG detection

strategies, including Naive CLS, Verification, and Anomaly Detection. Experimental results are reported in Table 1, Table 2 and Table 3, respectively. Our method achieves a significant performance improvement in all OOG percentages, but it also suffers slight performance degradation in the IG scenario. For instance, under the default evaluation protocol on the OUMVLP dataset, which includes 7% OOG queries, the accuracy of GaitGL combined with our method is 91.52%, slightly lower than the 92.27% accuracy achieved by GaitGL with the Naive CLS. We hypothesize that the primary reason for this discrepancy lies in the insufficiently discriminative feature space of the three backbones (*i.e.*, GaitSet, GaitPart, and GaitGL) across different subjects. Specifically, the lack of sufficient margins or distance between features for some challenging cases results in these samples being rejected by our method. Since our method prefers to accept matching pairs with minimal risk, these high-risk predictions are rejected and the overall accuracy drops in the IG case.

Performance across different datasets: We conduct experiments on three popular used datasets, *i.e.*, OUMVLP [5], CASIA-B [61], and Gait3D [10], to verify the effectiveness of our uncertainty gait recognition framework. Table 1, Table 2 and Table 3 demonstrate state-of-the-art backbones with our methods achieving superior performance in all OOG percentages. Additionally, for the default setting on the OUMVLP dataset, DyGait, with our method, achieves an accuracy of 99.00%. When the OOG percentage increases to 55%, our method still obtains 96.08% Rank-1 accuracy. The performance degradation on the OUMVLP dataset is only 3%. However, there is an obvious performance degradation on the CASIA-B dataset when the OOG percentage increases from 0% to 55%. We speculate that our method trained on a small dataset, like CASIA-B, which only contains 74 subjects for training, may not learn sufficiently discriminative features and thus suffer a performance drop in high OOG percentage.

For the Gait3D dataset, it is observed that the performance degrades about 10% as OOG percentage increases from 5% to 55%. The main reason is that existing methods cannot effectively extract discriminative features on Gait3D (the accuracy of these methods is lower than 50%). When the extracted features are not discriminative in handling IG queries, we do not expect these features to be robust enough to address OOG queries.

Extension to other tasks: To verify the applicability of our method to other tasks, we also conduct experiments on vehicle re-identification benchmark VERI-Wild [62], [63] and synthetic person-identification benchmark VC-Clothes [64]. The experimental details and results can be found in Table 5 and Table 6. These experiments demonstrate our uncertainty-aware model is able to effectively recognize matching feature pairs and OOG queries through its prediction and uncertainty modeling, thus demonstrating the superiority of our method to the state-of-the-art methods.

6 Conclusion

In this paper, we propose an Evidence-based Match-status-Aware Gait Recognition (EMA-GR) framework that can effectively identify whether a probe sample is out of the gallery samples. To the best of our knowledge, EMA-GR is the first attempt to endow gait recognition with the capability to address Out-of-Gallery (OOG) queries via uncertainty modeling. Furthermore, the proposed method is a unified framework that is not only able to address OOG query samples but also to successfully recognize identities of the In-Gallery (IG) samples. Since EMA-GR takes extracted gait features as input, it can be applied to various gait recognition networks, and thus agnostic against backbone networks. More importantly, EMA-GR can be generalized to other recognition tasks, such as vehicle and person re-identification, and improves the robustness of OOG queries, which frequently occur in practice.

Acknowledgments

This work was supported by the ARC-Discovery grant (DP220100800) and ARC-DECRA grant (DE230100477), the National Natural Science Foundation of China (61976017 and 61601021), the Beijing Natural Science Foundation (4202056), the Fundamental Research Funds for the Central Universities (2022JBMC013). The support and resources from the Center for High Performance Computing at Beijing Jiaotong University (http://hpc.bjtu.edu.cn) are gratefully acknowledged.

References

[1] C. Wan, L. Wang, and V. V. Phoha, "A survey on gait recognition," *ACM Computing Surveys (CSUR)*, vol. 51, no. 5, pp. 1–35, 2018.

[2] A. P. Dempster, "A generalization of bayesian inference," in *Classic Works of the Dempster-Shafer Theory of Belief Functions*, ser. Studies in Fuzziness and Soft Computing, R. R. Yager and L. Liu, Eds. Springer, 2008, vol. 219, pp. 73–104. [Online]. Available: https://doi.org/10.1007/978-3-540-44792-4_4

[3] M. Sensoy, L. Kaplan, and M. Kandemir, "Evidential deep learning to quantify classification uncertainty," *Advances in Neural Information Processing Systems*, vol. 31, 2018.

[4] M. Wang, X. Guo, B. Lin, T. Yang, Z. Zhu, L. Li, S. Zhang, and X. Yu, "Dygait: Exploiting dynamic representations for high-performance gait recognition," in *Proceedings of the IEEE/CVF Conference on Computer Vision and Pattern Recognition*, 2023.

[5] N. Takemura, Y. Makihara, D. Muramatsu, T. Echigo, and Y. Yagi, "Multi-view large population gait dataset and its performance evaluation for cross-view gait recognition," *IPSJ Transactions on Computer Vision and Applications*, vol. 10, no. 1, p. 4, 2018.

[6] A. Sepas-Moghaddam and A. Etemad, "Deep gait recognition: A survey," *IEEE Transactions on Pattern Analysis and Machine Intelligence*, 2022.

[7] C. Shen, S. Yu, J. Wang, G. Q. Huang, and L. Wang, "A comprehensive survey on deep gait recognition: Algorithms, datasets and challenges," *arXiv preprint arXiv:2206.13732*, 2022.

[8] S. Yu, Y. Huang, L. Wang, Y. Makihara, E. B. G. Reyes, F. Zheng, M. A. R. Ahad, B. Lin, Y. Yang, H. Xiong *et al.*, "Hid 2021: Competition on human identification at a distance 2021," in *2021 IEEE International Joint Conference on Biometrics (IJCB)*. IEEE, 2021, pp. 1–7.

[9] Z. Zhu, X. Guo, T. Yang, J. Huang, J. Deng, G. Huang, D. Du, J. Lu, and J. Zhou, "Gait recognition in the wild: A benchmark," in *ICCV*, 2021.

[10] J. Zheng, X. Liu, W. Liu, L. He, C. Yan, and T. Mei, "Gait recognition in the wild with dense 3d representations and a benchmark," in *Proceedings of the IEEE/CVF Conference on Computer Vision and Pattern Recognition*, 2022, pp. 20 228–20 237.

[11] S. Zhang, Y. Wang, and A. Li, "Cross-view gait recognition with deep universal linear embeddings," in *Proceedings of the IEEE/CVF Conference on Computer Vision and Pattern Recognition*, 2021, pp. 9095–9104.

[12] X. Li, Y. Makihara, C. Xu, and Y. Yagi, "Multi-view large population gait database with human meshes and its performance evaluation," *IEEE Transactions on Biometrics, Behavior, and Identity Science*, vol. 4, no. 2, pp. 234–248, 2022.

[13] D. K. Wagg and M. S. Nixon, "On automated model-based extraction and analysis of gait," in *CAFGR*, 2004.

[14] X. Li, Y. Makihara, C. Xu, Y. Yagi, S. Yu, and M. Ren, "End-to-end model-based gait recognition," in *ACCV*, 2020.

[15] X. Li, Y. Makihara, C. Xu, and Y. Yagi, "End-to-end model-based gait recognition using synchronized multi-view pose constraint," in *Proceedings of the IEEE/CVF International Conference on Computer Vision*, 2021, pp. 4106–4115.

[16] T. Teepe, A. Khan, J. Gilg, F. Herzog, S. Hörmann, and G. Rigoll, "Gaitgraph: Graph convolutional network for skeleton-based gait recognition," in *2021 IEEE International Conference on Image Processing (ICIP)*. IEEE, 2021, pp. 2314–2318.

[17] R. Liao, S. Yu, W. An, and Y. Huang, "A model-based gait recognition method with body pose and human prior knowledge," *Pattern Recognition*, vol. 98, p. 107069, 2020.

[18] H.-M. Hsu, Y. Wang, C.-Y. Yang, J.-N. Hwang, H. L. U. Thuc, and K.-J. Kim, "Gaittake: Gait recognition by temporal attention and keypoint-guided embedding," in *2022 IEEE International Conference on Image Processing (ICIP)*. IEEE, 2022, pp. 2546–2550.

[19] T. Teepe, J. Gilg, F. Herzog, S. Hörmann, and G. Rigoll, "Towards a deeper understanding of skeleton-based gait recognition," in *Proceedings of the IEEE/CVF Conference on Computer Vision and Pattern Recognition*, 2022, pp. 1569–1577.

[20] K. Shiraga, Y. Makihara, D. Muramatsu, T. Echigo, and Y. Yagi, "Geinet: View-invariant gait recognition using a convolutional neural network," in *ICB*. IEEE, 2016, pp. 1–8.

[21] X. Li, Y. Makihara, C. Xu, Y. Yagi, and M. Ren, "Gait recognition via semi-supervised disentangled representation learning to identity and covariate features," in *CVPR*, 2020.

[22] X. Wang and W. Q. Yan, "Human gait recognition based on frame-by-frame gait energy images and convolutional long short-term memory," *IJNS*, 2020.

[23] C. Shen, B. Lin, S. Zhang, X. Yu, G. Q. Huang, and S. Yu, "Gait recognition with mask-based regularization," in *IJCB*, 2023, pp. 1–10.

[24] B. Lin, Y. Liu, and S. Zhang, "Gaitmask: Mask-based model for gait recognition." BMVC, 2021.

[25] B. Lin, S. Zhang, and F. Bao, "Gait recognition with multiple-temporal-scale 3d convolutional neural network," in *Proceedings of the 28th ACM international conference on multimedia*, 2020, pp. 3054–3062.

[26] T. Chai, A. Li, S. Zhang, Z. Li, and Y. Wang, "Lagrange motion analysis and view embeddings for improved gait recognition," in *Proceedings of the IEEE/CVF Conference on Computer Vision and Pattern Recognition*, 2022, pp. 20 249–20 258.

[27] X. Huang, D. Zhu, H. Wang, X. Wang, B. Yang, B. He, W. Liu, and B. Feng, "Context-sensitive temporal feature learning for gait recognition," in *Proceedings of the IEEE/CVF International Conference on Computer Vision*, 2021, pp. 12 909–12 918.

[28] B. Lin, S. Zhang, M. Wang, L. Li, and X. Yu, "Gaitgl: Learning discriminative global-local feature representations for gait recognition," *arXiv preprint arXiv:2208.01380*, 2022.

[29] M. Wang, B. Lin, X. Guo, L. Li, Z. Zhu, J. Sun, S. Zhang, and X. Yu, "Gaitstrip: Gait recognition via effective strip-based feature representations and multi-level framework," *arXiv preprint arXiv:2203.03966*, 2022.

[30] B. Lin, S. Zhang, Y. Liu, and S. Qin, "Multi-scale temporal information extractor for gait recognition," in *2021 IEEE International Conference on Image Processing (ICIP)*. IEEE, 2021, pp. 2998–3002.

[31] W. Yu, H. Yu, Y. Huang, C. Cao, and L. Wang, "Cntn: Cyclic noise-tolerant network for gait recognition," *arXiv preprint arXiv:2210.06910*, 2022.

[32] W. Yu, H. Yu, Y. Huang, and L. Wang, "Generalized inter-class loss for gait recognition," in *Proceedings of the 30th ACM International Conference on Multimedia*, 2022, pp. 141–150.

[33] J. Liang, C. Fan, S. Hou, C. Shen, Y. Huang, and S. Yu, "Gaitedge: Beyond plain end-to-end gait recognition for better practicality," *arXiv preprint arXiv:2203.03972*, 2022.

[34] H. Dou, P. Zhang, Y. Zhao, L. Dong, Z. Qin, and X. Li, "Gaitmpl: Gait recognition with memory-augmented progressive learning," *IEEE Transactions on Image Processing*, 2022.

[35] H. Dou, P. Zhang, W. Su, Y. Yu, and X. Li, "Metagait: Learning to learn an omni sample adaptive representation for gait recognition," in *European Conference on Computer Vision*. Springer, 2022, pp. 357–374.

[36] T. Huang, X. Ben, C. Gong, B. Zhang, R. Yan, and Q. Wu, "Enhanced spatial-temporal salience for cross-view gait recognition," *IEEE Transactions on Circuits and Systems for Video Technology*, 2022.

[37] S. Hou, X. Liu, C. Cao, and Y. Huang, "Set residual network for silhouette-based gait recognition," *IEEE Transactions on Biometrics, Behavior, and Identity Science*, vol. 3, no. 3, pp. 384–393, 2021.

[38] S. Hou, C. Cao, X. Liu, and Y. Huang, "Gait lateral network: Learning discriminative and compact representations for gait recognition," in *European conference on computer vision*. Springer, 2020, pp. 382–398.

[39] Z. Huang, D. Xue, X. Shen, X. Tian, H. Li, J. Huang, and X.-S. Hua, "3d local convolutional neural networks for gait recognition," in *CVPR*, 2021, pp. 14 920–14 929.

[40] X. Zhu, Z. Luo, P. Fu, and X. Ji, "Voc-reid: Vehicle re-identification based on vehicle-orientation-camera," in *CVPR Workshops*, 2020, pp. 602–603.

[41] Z. Tang, M. Naphade, M.-Y. Liu, X. Yang, S. Birchfield, S. Wang, R. Kumar, D. Anastasiu, and J.-N. Hwang, "Cityflow: A city-scale benchmark for multi-target multi-camera vehicle tracking and re-identification," in *Proceedings of the IEEE/CVF Conference on Computer Vision and Pattern Recognition*, 2019, pp. 8797–8806.

[42] V. Devyatkov, A. Alfimtsev, and A. Taranyan, "Multicamera human re-identification based on covariance descriptor," *Pattern Recognition and Image Analysis*, vol. 28, no. 2, pp. 232–242, 2018.

[43] J. Guo, X. Zhu, C. Zhao, D. Cao, Z. Lei, and S. Z. Li, "Learning meta face recognition in unseen domains," in *Proceedings of the IEEE/CVF Conference on Computer Vision and Pattern Recognition*, 2020, pp. 6163–6172.

[44] M. M. Kalayeh, E. Basaran, M. Gökmen, M. E. Kamasak, and M. Shah, "Human semantic parsing for person re-identification," in *Proceedings of the IEEE conference on computer vision and pattern recognition*, 2018, pp. 1062–1071.

[45] W. J. Scheirer, A. de Rezende Rocha, A. Sapkota, and T. E. Boult, "Toward open set recognition," *IEEE transactions on pattern analysis and machine intelligence*, vol. 35, no. 7, pp. 1757–1772, 2012.

[46] W. Bao, Q. Yu, and Y. Kong, "Evidential deep learning for open set action recognition," in *Proceedings of the IEEE/CVF International Conference on Computer Vision*, 2021, pp. 13 349–13 358.

[47] Y. Gal and Z. Ghahramani, "Dropout as a bayesian approximation: Representing model uncertainty in deep learning." PMLR, 2016, pp. 1050–1059.

[48] D. Molchanov, A. Ashukha, and D. Vetrov, "Variational dropout sparsifies deep neural networks," in *International Conference on Machine Learning*. PMLR, 2017, pp. 2498–2507.

[49] Y. Gal, J. Hron, and A. Kendall, "Concrete dropout," *Advances in neural information processing systems*, vol. 30, 2017.

[50] A. Amini, A. Soleimany, S. Karaman, and D. Rus, "Spatial uncertainty sampling for end-to-end control," *arXiv preprint arXiv:1805.04829*, 2018.

[51] T. Pearce, F. Leibfried, and A. Brintrup, "Uncertainty in neural networks: Approximately bayesian ensembling," in *The 23rd International Conference on Artificial Intelligence and Statistics, AISTATS 2020*, ser. Proceedings of Machine Learning Research, vol. 108. PMLR, 2020, pp. 234–244.

[52] B. Lakshminarayanan, A. Pritzel, and C. Blundell, "Simple and scalable predictive uncertainty estimation using deep ensembles," *Advances in neural information processing systems*, vol. 30, 2017.

[53] C. Blundell, J. Cornebise, K. Kavukcuoglu, and D. Wierstra, "Weight uncertainty in neural network," in *International conference on machine learning*. PMLR, 2015, pp. 1613–1622.

[54] J. M. Hernández-Lobato and R. Adams, "Probabilistic backpropagation for scalable learning of bayesian neural networks," in *International conference on machine learning*. PMLR, 2015, pp. 1861–1869.

[55] A. Gelman, "Prior distributions for variance parameters in hierarchical models (comment on article by browne and draper)," *Bayesian analysis*, vol. 1, no. 3, pp. 515–534, 2006.

[56] A. Gelman, A. Jakulin, M. G. Pittau, and Y.-S. Su, "A weakly informative default prior distribution for logistic and other regression models," *The annals of applied statistics*, vol. 2, no. 4, pp. 1360–1383, 2008.

[57] A. Malinin and M. Gales, "Predictive uncertainty estimation via prior networks," *Advances in neural information processing systems*, vol. 31, 2018.

[58] A. Malinin and M. J. F. Gales, "Reverse kl-divergence training of prior networks: Improved uncertainty and adversarial robustness," in *Advances in Neural Information Processing Systems 2019*, 2019, pp. 14 520–14 531.

[59] S. Kotz, N. Balakrishnan, and N. L. Johnson, *Continuous multivariate distributions, Volume 1: Models and applications*. John Wiley & Sons, 2004, vol. 1.

[60] A. P. Dempster, *Classic works of the Dempster-Shafer theory of belief functions*, 2008.

[61] S. Yu, D. Tan, and T. Tan, "A framework for evaluating the effect of view angle, clothing and carrying condition on gait recognition," in *ICPR*, vol. 4. IEEE, 2006, pp. 441–444.

[62] Y. Lou, Y. Bai, J. Liu, S. Wang, and L.-Y. Duan, "Veri-wild: A large dataset and a new method for vehicle re-identification in the wild," in *CVPR*, 2019, pp. 3235–3243.

[63] Y. Bai, J. Liu, Y. Lou, C. Wang, and L.-Y. Duan, "Disentangled feature learning network and a comprehensive benchmark for vehicle re-identification," in *In IEEE Transactions on Pattern Analysis and Machine Intelligence*, 2021.

[64] F. Wan, Y. Wu, X. Qian, Y. Chen, and Y. Fu, "When person re-identification meets changing clothes," in *Proceedings of the IEEE/CVF Conference on Computer Vision and Pattern Recognition Workshops*, 2020, pp. 830–831.

[65] H. Chao, Y. He, J. Zhang, and J. Feng, "Gaitset: Regarding gait as a set for cross-view gait recognition," in *Proceedings of the AAAI conference on artificial intelligence*, vol. 33, no. 01, 2019, pp. 8126–8133.
[66] C. Fan, Y. Peng, C. Cao, X. Liu, S. Hou, J. Chi, Y. Huang, Q. Li, and Z. He, "Gaitpart: Temporal part-based model for gait recognition," in *Proceedings of the IEEE/CVF Conference on Computer Vision and Pattern Recognition*, 2020, pp. 14 225–14 233.
[67] B. Lin, S. Zhang, and X. Yu, "Gait recognition via effective global-local feature representation and local temporal aggregation," in *ICCV*, 2021, pp. 14 648–14 656.
[68] L. He, X. Liao, W. Liu, X. Liu, P. Cheng, and T. Mei, "Fastreid: A pytorch toolbox for general instance re-identification," *arXiv preprint arXiv:2006.02631*, 2020.
[69] C. Fan, J. Liang, C. Shen, S. Hou, Y. Huang, and S. Yu, "Opengait: Revisiting gait recognition towards better practicality," in *CVPR*, 2023.
[70] H. Luo, Y. Gu, X. Liao, S. Lai, and W. Jiang, "Bag of tricks and a strong baseline for deep person re-identification," in *CVPR workshops*, 2019, pp. 0–0.
[71] Z. Zhuang, L. Wei, L. Xie, T. Zhang, H. Zhang, H. Wu, H. Ai, and Q. Tian, "Rethinking the distribution gap of person re-identification with camera-based batch normalization," in *ECCV*, 2020, pp. 140–157.
[72] J. Yang, K. Zhou, Y. Li, and Z. Liu, "Generalized out-of-distribution detection: A survey," *arXiv preprint arXiv:2110.11334*, 2021.